論文 / 著書情報
Article / Book Information

Title	RESPONSE PREDICTION METHOD FOR FLEXIBLE-STIFF MIXED STRUCTURE WITH DISPLACEMENT CONTROLLER BASED ON ENERGY BALANCE
Authors	Jing LI, D. Sato, N. Nomura, H. Kitamura, T. Ueki, K. Miyagawa
Pub. date	2020, 9
Citation	2020 17WCEE Proceedings

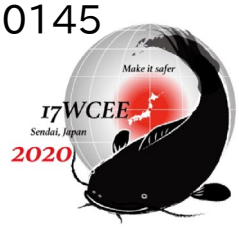

17th World Conference on Earthquake Engineering, 17WCEE
Sendai, Japan - September 13th to 18th 2020

RESPONSE PREDICTION METHOD FOR FLEXIBLE-STIFF MIXED STRUCTURE WITH DISPLACEMENT CONTROLLER BASED ON ENERGY BALANCE

J. Li[(1)], D. Sato[(2)], N. Nomura[(3)], H. Kitamura[(4)], T. Ueki[(5)], K. Miyagawa[(6)]

[(1)] *Research student, Tokyo Institute of Technology, Japan. Email: rishou2019@yahoo.co.jp*
[(2)] *Associate professor, Tokyo Institute of Technology, Japan.*
[(3)] *Former Graduate student, Tokyo University of Science, Japan.*
[(4)] *Vice president, Tokyo University of Science, Japan.*
[(5)] *JFE Steel Corporation*
[(6)] *JFE Civil engineering & Construction Corporation*

Abstract

Traditional structures are easy to be plasticized under huge earthquakes, thus losing their functions. Therefore, flexible-stiff mixed structures have been developed to absorb seismic energy. However, in huge earthquakes, flexible-stiff mixed structures often have the possibility of displacement exceeding the limit, so people develop displacement controller to solve this problem. Recent research on the displacement controller has been proven that the displacement controller which has hardening type hysteresis can reduce the displacement of frame or isolation layer against the huge earthquake from many experimental or analytical results. However, it is difficult to qualitatively evaluate changes in various parameters. Therefore, the purpose of this paper is to qualitatively and simply evaluate the response characteristics of the flexible-stiff mixed structure with displacement controller.

In this paper, we used energy balance-based seismic response prediction method proposed by Prof Akiyama and extended the structure with displacement controller. Then the result of response prediction method was confirmed by many time history response analyses using the single-degree-of-freedom (SDOF) model. In addition, we used response prediction method for the isolated structure with displacement controller and analyze the results of the discussion.

From the prediction formula, we can know that the bigger the stiffness of the displacement controller, the smaller the deformation when the displacement controller starts working, and the more obvious the reduction of the maximum deformation. And the bigger the stiffness of the displacement controller, the more obvious the increase of the maximum shear force. For the SDOF model of the isolated structure with displacement controller structure, the response characteristics can be evaluated based on the predicted values and the analytical values of the SDOF. When the amount of damper increases, the maximum deformation of the structure can be reduced in huge earthquakes, but when the displacement controller starts to work, the maximum shear force increases with the decrease of the maximum deformation. When the amount of damper is increased, the efficiency of the damper is low in small earthquakes. Therefore, the combination of structures should be selected appropriately.

Keywords: Displacement Controller, Huge Earthquake, Flexible-Stiff Mixed Structure, SDOF Model, Energy Balance,

Response Prediction Method

1. Introduction

The conventional seismic design is based on the idea of avoiding collapse of buildings by absorbing seismic energy through plasticization of their main frame and thus protecting human lives. However, this design has several problems, such as loss of building function due to plasticization of the main frame and the seismic resistance of the building being governed by the energy absorption capacity of some elements or layers. These problems can be resolved by adopting a flexible–stiff mixed structure [1] [2] composed of a flexible element that performs elastic behavior with slight stiffness and a stiff element that performs elastic-plastic behavior with great stiffness and absorbs the input seismic energy. The adoption of a flexible–stiff mixed structure has not only been found to enable rational seismic design, but also reduce damage to the main frame, thus facilitating retrofitting after an earthquake.

In 1995, buildings were significantly damaged owing to Hyogoken Nanto earthquake, a maximal earthquake that caused a 7-class earthquake motion [3]. In 2011, a 9.0 maximum magnitude earthquake occurred in the east-north Region Pacific Coast of Japan [4]. In recent years, the occurrence of several maximal earthquakes, such as the Nankai Trough [5] , Tokyo metropolitan area [6], and Uemachi fault earthquakes, has caused concerns, as they are expected to have caused significant damage in urban areas. For earthquakes that exceed the above-mentioned conventional assumed levels, buildings [7] having higher earthquake resistance have been attracting attention for the purpose of maintaining the structure functions. Thus, the importance of introducing a displacement controller is increasing.

Various studies have been carried out on displacement controllers. Kobori et al. [8] proposed a system having hardening type restoring force characteristics by considering the nonlinear theory and showed the possibility of a new type of seismic structure by conducting analytical examination. Takahashi et al. [9] reduced the maximum deformation during earthquakes by incorporating a horizontal displacement control device that acted from a certain displacement onto the seismic isolation layer to control its excessive response that occurs during large earthquakes. Experiments and response analysis carried out in the study showed that that the damage to the superstructure can be suppressed to an extent, where furniture also did not topple. Furthermore, Iiba et al. [10] focused on a base-isolated house, where the clearance of the base-isolation layer was not sufficiently large, and assessed the impact of the base-isolation layer on the response of the superstructure by conducting the shaking table experiment. By using the response analysis results that changed the earthquake motion, a seismic isolation system and a displacement restraining member, with a displacement restraining design method for a detached house was proposed.

In above-mentioned studies, it was experimentally and analytically shown that maximum deformation of the isolation layer in the frame and base isolation structure, during extreme earthquakes, can be reduced by incorporating a displacement controller with hardening–type restoring force characteristic. However, it is difficult to qualitatively evaluate the change in the response characteristics using various parameters. Therefore, the purpose of this study was to qualitatively and easily evaluate the response characteristics of a displacement controller structure that incorporated a displacement controller, with hardening-type restoring force characteristics, into a seismic isolation structure used in a building exhibiting advanced seismic performance. We extended the seismic design method [13], based on the energy balance proposed by Akiyama for a Single Degree of Freedom model, to a displacement controller structure that incorporated the displacement controller, with hardening-type restoring force characteristics, in a flexible–stiff mixed structure, and proposed an energy method for the displacement controller structure. In addition, the response prediction formula was verified using the time history response analysis.

2. Proposed energy method with the displacement controller

2.1 Outline of the displacement controller

Fig. 1 shows the hysteretic curve of the displacement controller, and Fig. 2 shows the analysis model of SDOF. The displacement controller consisted of a flexible element, a stiff element, and a displacement controller. The flexible element supported the gravity of the building and was in elastic deformation. The

stiff element absorbed the seismic energy and had an elastic-plastic behavior. The displacement controller exhibited a hardening hysteresis curve from a certain deformation. We discuss the working ($\delta_{\max} > {}_d\delta_{gap}$) (Fig. 1 (b)) and not working ($\delta_{\max} < {}_d\delta_{gap}$) (Fig. 1 (a)) hysteresis curve of the displacement controller, separately. Here, δ_{max} and ${}_d\delta_{gap}$ represent the maximum deformation and deformation at which the displacement controller started to work, respectively. Assuming the flexible element and displacement controller are in elastic deformation. The stiff element exhibited elastic-plastic behavior. In addition, ${}_d\delta_{gap}$ was found to be larger than the yield deformation of the stiff element ${}_s\delta_y$ (${}_d\delta_{gap} > {}_s\delta_y$). In addition, all the deformation contributed to the deformation of the stiff element, and it was necessary to separately consider the influence of the entire bending deformation, which impaired the transmission of the stiff element deformation [14].

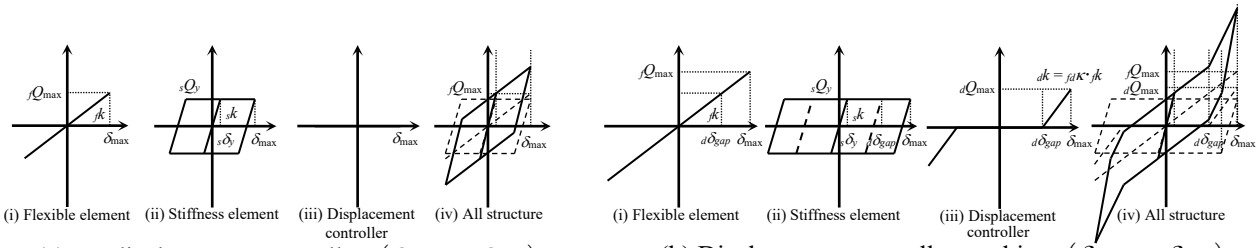

(a) No displacement controller ($\delta_{\max} < {}_d\delta_{gap}$) (b) Displacement controller working ($\delta_{\max} > {}_d\delta_{gap}$)

Fig. 1 – Hysteretic behavior of displacement controller

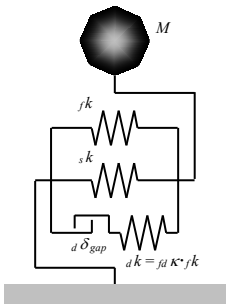

Fig. 2 – Analytical model

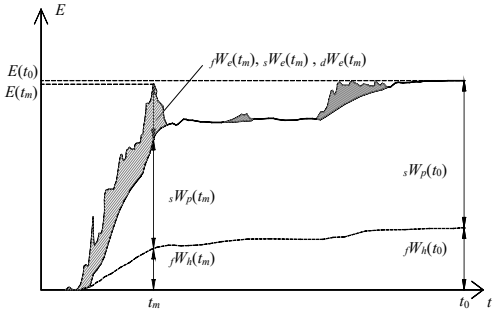

Fig. 3 – Historic response of energy

2.2 Derivation of the response prediction formula in the displacement controller

Fig. 3 shows the energy time history response in the displacement controller. The horizontal axis shows the starting time of earthquake as t. Here, t_m and t_0 represent the maximum response value occurring time of a building and duration of the earthquake motion, respectively. ${}_fW_e(t)$ and ${}_fW_h(t)$ represent the elastic vibration energy of the flexible element and energy consumed by damping, respectively. ${}_sW_e(t)$ and ${}_sW_p(t)$ represent the elastic vibration energy and plastic hysteresis energy of the stiff element, respectively, and ${}_dW_e(t)$ represent the elastic vibration energy of the displacement controller. It can be observed from Fig. 3 that ${}_fW_e(t)$, ${}_sW_e(t)$, and ${}_dW_e(t)$ exhibited maximum values at $t = t_m$ and almost disappeared at $t = t_0$. Further, $E(t)$ represents the input energy and $E(t) - {}_fW_h(t)$ is defined damage energy $E_D(t)$ [12].

As the purpose of the displacement controller structure was to control the occurrence of excessive deformation in case of maximal earthquakes, in this study, we considered the energy balance [14] by focusing on the maximum response value generation time t_m. The displacement controller structure has been noted to prevent excessive deformation in case of large earthquakes. In the base-isolated structure, the ratio of plastic and reducing energies of the base-isolated and seismic control members to the input energy was found to increase, and was mostly found to be $E(t_m) \le E(t_0)$. As the evaluation of input ergonomics was connected to the evaluation of the safety side of the response, if $E_D(t_m)$ is replaced with $E_D(t_0)$ in the displacement controller structure, the formula for $t = t_m$ can be expressed as follows:

$$\begin{aligned} {}_fW_e(t_m) + {}_sW_p(t_m) &= E_D(t_0) && (\delta_{max} < {}_d\delta_{gap}) \\ {}_fW_e(t_m) + {}_sW_p(t_m) + {}_dW_e(t_m) &= E_D(t_0) && (\delta_{max} < {}_d\delta_{gap}) \end{aligned} \quad (1a, b)$$

Here, ${}_sW_e(t_m)$ can be ignored, as it is significantly smaller than $E_D(t_0)$ [14].

Subsequently, the SDOF system model was used as the object to express the energy equation for each element of equation (1).

The equation for the damage causing energy $E_D(t_0)$ is as follows [12]:

$$E_D(t_0) = \frac{M \cdot V_D^2}{2} \tag{2}$$

Here, M: mass and V_D: velocity conversion value [12] of E_D.

The equation for the elastic vibration energy of the flexible element ${}_fW_e(t_m)$ is as follows:

$${}_fW_e(t_m) = \frac{{}_fQ_{\max} \cdot \delta_{\max}}{2} = \frac{{}_fQ_{\max}{}^2}{2 \cdot {}_fk} = \frac{\left({}_f\alpha_{\max} \cdot M \cdot g\right)^2}{2} \frac{{}_fT_1^2}{4\pi^2 \cdot M} = \frac{M \cdot V_D^2}{2} \left(\frac{{}_f\alpha_{\max}}{{}_f\alpha_0} \right)^2 \tag{3}$$

$$\text{Here, } \delta_{\max} = \frac{{}_fQ_{\max}}{{}_fk},\ {}_f\alpha_{\max} = \frac{{}_fQ_{\max}}{M \cdot g},\ {}_fk = \frac{4\pi^2 \cdot M}{{}_fT_1{}^2},\ {}_f\alpha_0 = \frac{2\pi \cdot V_D}{{}_fT_1 \cdot g} \tag{4a–d}$$

Here, ${}_fQ_{\max}$: maximum sheer force of the flexible element, $\delta_{\max}$: maximum deformation, ${}_fk$: flexible element stiffness, g: gravitational acceleration, ${}_f\alpha_{\max}$: maximum shear coefficient of the flexible element, ${}_fT_1$: first time natural period for only the flexible element, and ${}_f\alpha_0$: maximum shear force coefficient of only the flexible element.

The plastic hysteresis energy of the stiff element ${}_sW_p(t_m)$ is expressed by the following equation, using the equivalent repetitions number n_1 of the stiff element.

$$\begin{aligned} {}_sW_p(t_m) &= 4n_1 \cdot {}_sQ_y \cdot (\delta_{\max} - {}_s\delta_y) \cong 4n_1 \cdot {}_sQ_y \cdot \delta_{\max} = 4n_1 \cdot \frac{{}_sQ_y \cdot {}_fQ_{\max}}{{}_fk} \\ &= 4n_1 \cdot \left({}_s\alpha_y \cdot M \cdot g\right) \cdot \left({}_f\alpha_{\max} \cdot M \cdot g\right) \frac{{}_fT_1^2}{4\pi^2 \cdot M} = \frac{M \cdot V_D^2}{2} \cdot 8n_1 \cdot \left(\frac{{}_s\alpha_y}{{}_f\alpha_0} \right) \left(\frac{{}_f\alpha_{\max}}{{}_f\alpha_0} \right) \end{aligned} \tag{5}$$

$$\text{Here, } \delta_{\max} - {}_s\delta_y \cong \delta_{\max},\ {}_s\alpha_y = \frac{{}_sQ_y}{M \cdot g} \tag{6a–b}$$

Here, ${}_sQ_y$: yield shear of the stiff element, ${}_s\delta_y$: yield deformation of the stiff element, and ${}_s\alpha_y$: yield shear coefficient of the stiff element. It was expected that the energy absorption efficiency of the stiff element would decrease, owing to the action of the deformation controller. However, as the displacement controller working duration was shorter than the seismic motion duration, the same n_1 is used in this paper regardless of the presence or absence of the displacement controller.

The elastic vibration energy of the displacement controller ${}_dW_e(t_m)$ is expressed by the following equation.

$${}_dW_e(t_m) = \frac{{}_dQ_{\max} \cdot \left(\delta_{\max} - {}_d\delta_{gap}\right)}{2} = \frac{{}_dQ_{\max}^2}{2 \cdot {}_dk} = \frac{M \cdot V_D^2}{2 \cdot {}_{fd}\kappa} \cdot \left(\frac{{}_d\alpha_{\max}}{{}_f\alpha_0} \right)^2 \tag{7}$$

$$\text{Here, } {}_dk = \frac{{}_dQ_{\max}}{\delta_{\max} - {}_d\delta_{gap}},\ {}_d\alpha_{\max} = \frac{{}_dQ_{\max}}{M \cdot g},\ {}_{fd}\kappa = {}_dk / {}_fk \tag{8a–c}$$

Here, ${}_dQ_{\max}$: maximum shear of the displacement controller, ${}_d\delta_{gap}$: deformation at which the displacement controller starts to work, ${}_dk$: stiffness of the displacement controller, ${}_d\alpha_{\max}$: maximum shear coefficient of the displacement controller, and ${}_{fd}\kappa$: proportion of ${}_fk$ to ${}_dk$. Substituting equations (4a) and (8a) into equation (8c) and solving for ${}_d\alpha_{\max} / {}_f\alpha_0$, following equation is obtained.

$$\frac{{}_d\alpha_{\max}}{{}_f\alpha_0} = {}_{fd}\kappa \cdot \left(\frac{{}_f\alpha_{\max}}{{}_f\alpha_0} - \frac{{}_d\delta_{gap}}{{}_f\delta_0} \right) \tag{9}$$

Here, $${}_f\delta_0 = \frac{{}_fT_1 \cdot V_D}{2\pi} \tag{10}$$

Here, ${}_f\delta_0$: maximum deformation for only the flexible element. By substituting equation (9) into equation (7), ${}_dW_e(t_m)$ is finally expressed by the following equation.

$${}_dW_e(t_m) = \frac{M \cdot V_D^2}{2} \cdot {}_{fd}\kappa \cdot \left(\frac{{}_f\alpha_{\max}}{{}_f\alpha_0} - \frac{{}_d\delta_{gap}}{{}_f\delta_0} \right)^2 \tag{11}$$

Further, the response prediction formula is derived when the displacement controller works. By substituting the energy of each element of equations (2), (3), (5), and (11) into equation (1b), the following equation is obtained.

$$\left(\frac{{}_f\alpha_{\max}}{{}_f\alpha_0} \right)^2 + 8n_1 \cdot \left(\frac{{}_s\alpha_y}{{}_f\alpha_0} \right) \left(\frac{{}_f\alpha_{\max}}{{}_f\alpha_0} \right) + {}_{fd}\kappa \cdot \left(\frac{{}_f\alpha_{\max}}{{}_f\alpha_0} - \frac{{}_d\delta_{gap}}{{}_f\delta_0} \right)^2 = 1 \tag{12}$$

Here, $\delta_{\max} < {}_f\delta_0$ is expressed by the following equation by substituting equations (4b) and (4c) into equation (4a) and dividing it by equation (10).

$$\frac{\delta_{\max}}{{}_f\delta_0} = \frac{{}_f\alpha_{\max} \cdot M \cdot g \cdot {}_fT_1^2}{4\pi^2 \cdot M} \cdot \frac{2\pi}{{}_fT_1 \cdot V_D} = \frac{{}_f\alpha_{\max}}{{}_f\alpha_0} \tag{13}$$

Moreover, the relationship between the shear coefficient of each element and yield shear coefficient of the stiff element was derived. If equation (12) is solved for ${}_f\alpha_{\max} / {}_f\alpha_0$ ($= \delta_{\max} / {}_f\delta_0$), the following equation is obtained.

$$\frac{{}_f\alpha_{\max}}{{}_f\alpha_0} = \frac{\delta_{\max}}{{}_f\delta_0} = \frac{1}{1 + {}_{fd}\kappa} \left[\begin{array}{l} -4n_1 \cdot \dfrac{{}_s\alpha_y}{{}_f\alpha_0} + {}_{fd}\kappa \cdot \dfrac{{}_d\delta_{gap}}{{}_f\delta_0} \\ + \sqrt{\left(4n_1 \cdot \dfrac{{}_s\alpha_y}{{}_f\alpha_0} \right)^2 + 1 - 8\,{}_{fd}\kappa \cdot n_1 \cdot \dfrac{{}_d\delta_{gap}}{{}_f\delta_0} \cdot \dfrac{{}_s\alpha_y}{{}_f\alpha_0} + {}_{fd}\kappa \cdot \left\{ 1 - \left(\dfrac{{}_d\delta_{gap}}{{}_f\delta_0} \right)^2 \right\}} \end{array} \right] \tag{14}$$

From equation (14), the maximum shear coefficient for all structures $\alpha_{\max}$ divided by ${}_f\alpha_0$, $\alpha_{\max} / {}_f\alpha_0$ is expressed as follows:

$$\begin{aligned} \frac{\alpha_{\max}}{{}_f\alpha_0} &= \frac{{}_f\alpha_{\max}}{{}_f\alpha_0} + \frac{{}_s\alpha_y}{{}_f\alpha_0} + \frac{{}_d\alpha_{\max}}{{}_f\alpha_0} \\ &= -(4n_1 - 1) \cdot \frac{{}_s\alpha_y}{{}_f\alpha_0} + \sqrt{\left(4n_1 \cdot \frac{{}_s\alpha_y}{{}_f\alpha_0} \right)^2 + 1 - 8\,{}_{fd}\kappa \cdot n_1 \cdot \frac{{}_d\delta_{gap}}{{}_f\delta_0} \cdot \frac{{}_s\alpha_y}{{}_f\alpha_0} + {}_{fd}\kappa \cdot \left\{ 1 - \left(\frac{{}_d\delta_{gap}}{{}_f\delta_0} \right)^2 \right\}} \end{aligned} \tag{15}$$

Substituting equation (13) into equation (12) and solving for ${}_s\alpha_y / {}_f\alpha_0$ and $\alpha_{\max} / {}_f\alpha_0$, the relationship between the shear coefficient of each element and maximum deformation is derived. If ${}_{fd}\kappa = 0$ is used in the equations (12), (14), and (15), a response prediction formula for when the displacement controller does not work is derived. It was found to be consistent with the response prediction formula of the flexible–stiff mixed structure.

3. Verification of response prediction formula by time history response analysis

3.1 Analysis model and outline of the input ground motion

The response prediction formula, derived in the previous section, was verified using the time history response analysis of the displacement controller structure model, with the displacement controller. This paper presents the base-isolated structure model by considering SDOF as the object. The flexible element in the base isolated structure model was rubber. Table 1 shows the analytical parameters. The time history response analysis was carried out for the SDOF system model, with mass M: 100 tons, ${}_f T_1$: flexible element 1 natural period, ${}_s \alpha_y$: yield stiffness of the stiff element, ${}_d \delta_{gap} / {}_s \delta_0$: deformation at which the displacement controller starts working, ${}_f k$: stiffness of the flexible element, ${}_d k$: stiffness of the displacement controller, ${}_{fd} \kappa$: proportion of ${}_f k$ to ${}_d k$, E_D: damage causing energy, and V_D: velocity conversion value of E_D.

In this paper, it is assumed that the base isolation structure model installs a viscous damping type damper in the seismic isolation layer. The damping of the analytical model was set using the stiffness-proportional damping type, with ${}_f h = 0.02$, for the period of the flexible element ${}_f T_1$.

For the base isolation structure model, we assume that ${}_f T_1 = 3.0$, 4.0 s and set ${}_s \alpha_y = 0.01$–0.10, ${}_d \delta_{gap} / {}_f \delta_0 = 0.2$, 0.4, and ${}_{fd} \kappa = 20$. We assume the use of rigid dampers, such that the yield deformation ${}_s \delta_y$ is 27.9 mm [16]. The stiffness of the main frame ${}_f k = 0.439 \times 10^3$ KN/m and the stiffness of the displacement controller ${}_d k = 8.78 \times 10^3$ KN/m for 1 natural Period ${}_f T_1 = 3.0$ s.

Table 1 – Analytical parameter

${}_f T_1$	${}_s \alpha_y$	${}_d \delta_{gap} / {}_s \delta_y$	${}_f k$	V_D	
3.0, 4.0	0.01, 0.02, 0.04, 0.06, 0.10	0.2,0.4	20.0	ART KOBE	ART SHIN
				100, 200, 300	250, 500, 750

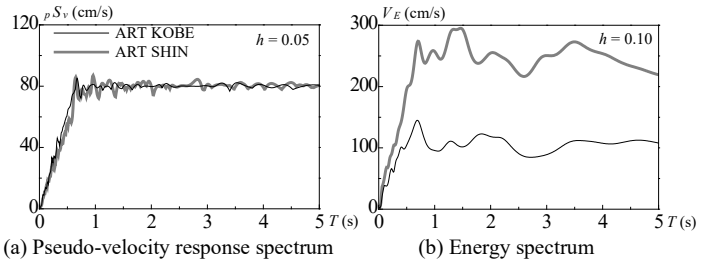

(a) Pseudo-velocity response spectrum (b) Energy spectrum

Fig. 4 – Earthquake ground response spectra

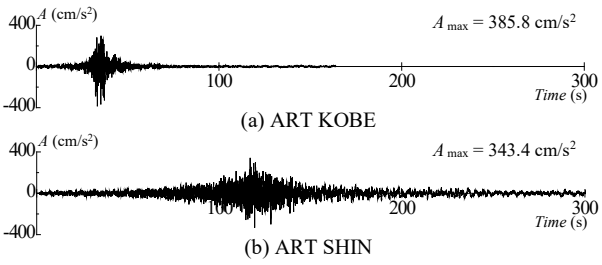

Fig. 5 – Ground motion wave (${}_p S_v = 80$ cm/s)

Fig. 4 shows the pseudo-velocity response spectrum ${}_p S_v$ (h = 0.05) of the ground motion and the energy spectrum V_E (h = 0.10). Fig. 5 shows the acceleration time history of the ground motion. For the input ground motion, a simulated wave created to match the announcement spectrum was used, and ${}_p S_v$ was set as constant at a corner period $T_c > 0.64$ s. The phase characteristic was JMA KOBE 1995 NS, which has been mostly used while designing high-rise and seismic isolation buildings, because of the large maximum response value and K-net observation point was the observation wave at Shinjuku district (TKY007) during the Tokyo Metropolitan earthquake. And we named them ART KOBE and ART SHIN respectively. Fig. 4 and 5 show the case where ${}_p S_v$ was constant at 80 cm/s. In this analysis, the velocity conversion value of the energy contributing to the damage in ART KOBE, V_D = 100 cm/s, was defined as an extremely rare ground motion level, with V_D = 100, 200, and 300 cm/s being used as parameters. In ART SHIN, V_D = 250 cm/s was defined as a very rare ground motion level, with V_D = 250, 500, and 750 cm/s being used as parameters. Table 1 shows the analysis parameters. In each case, the analysis was performed by adjusting the input acceleration magnification, such that the analysis value of the speed conversion V_D of the energy contributing to the

damage was approximately the same as V_D shown in Table 1.

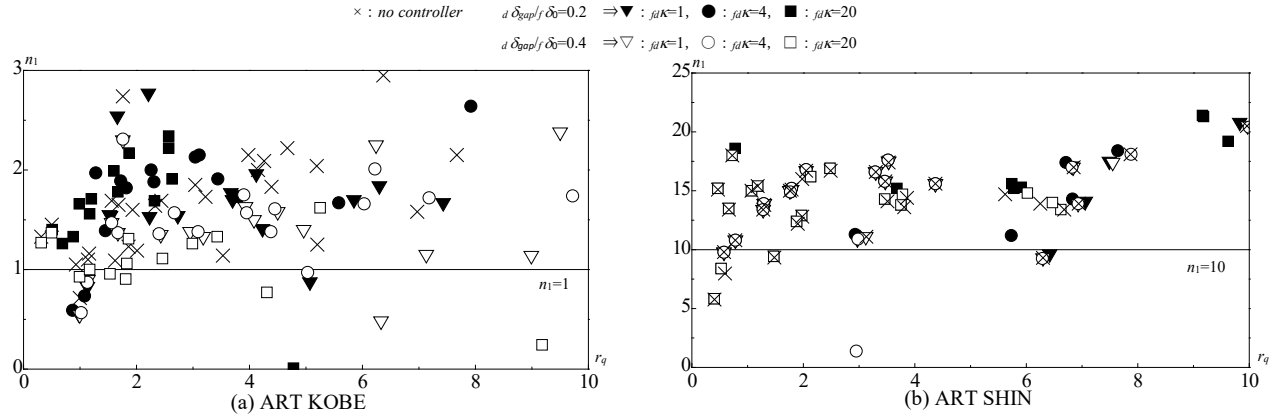

Fig. 6 – Relationship of n_1 and r_q

3.2 Comparison of the Analytical and Predicted Values and Discussion on the Response Prediction Formula

The predicted value obtained from the response prediction formula derived in Section 2.2 and the analysis value obtained from the time history response analysis carried out in the SDOF system model are compared in this paper. The response prediction formula, when the displacement controller works (equation (14) and (15)), was confirmed in this study. When the displacement controller was not incorporated in the analysis parameters shown in Table 1, the analysis was performed using the simulated waves, where the maximum accelerations were 1.0, 2.0, and 3.0 times the level 2 ground motion. The equivalent repetition number n_1 was observed to increase in proportion to the duration of the earthquake motion. In the based isolation structure, n_1 = 2.0 was set as the lower limit of EL CENTRO NS [12]. Here, we adopted short duration ground motion ART KOBE and long duration ground motion ART SHIN. Thus, n_1 is obtained from the analysis result of each ground motion using the analysis parameters mentioned in Table 1, and n_1 is adopted for calculating the predicted value based on the result. The analysis result is substituted into the following equation to find the equivalent repetition number n_1.

$$n_1 = \frac{E_D(t_0) - \{{}_fW_e(t_m) + {}_dW_e(t_m)\}}{4\,{}_sQ_y \cdot (\delta_{\max} - {}_s\delta_y)} \tag{16}$$

Fig. 6(a) and 6(b) show the relationship between r_q [13], which is the ratio of the maximum shear ${}_fQ_{\max}$ of the flexible element and the yield shear force ${}_sQ_y$ of the stiff element, and the equivalent repetition number n_1. As shown in Fig. 6(a), n_1 of ART KOBE was distributed in a range of approximately 1.0 to 3.0, when r_q was 1.0 or more. Thus, the lower limit of n_1 = 1.0 was adopted. Further, as shown in Fig. 6(b), n_1 of ART SHIN was distributed in a range of approximately 10 to 20, when r_q was 1.0 or more. Thus, the lower limit of n_1 = 10 was adopted. Subsequently, we adopted ${}_s\alpha_y$ as the parameter to calculate the predicted values $\delta_{\max}/\delta_0$ (= ${}_f\alpha_{\max}/{}_f\alpha_0$) and $\alpha_{\max}/\alpha_0$ using equations and (15), respectively.

Fig. 7(a) and 7(b) show the relationship between $\alpha_{\max}/\alpha_0$ and ${}_s\alpha_y/{}_f\alpha_0$ obtained using equation (15), with the parameters shown in Table 1. The thick dashed line represented $\alpha_{\max}/{}_f\alpha_0$, when the displacement controller was not incorporated and was denoted as no controller. The monotonously increasing thin solid line in the upper right part represented ${}_s\alpha_y/{}_f\alpha_0$, and the decreasing thin solid line in the lower right part represented ${}_f\alpha_{\max}/{}_f\alpha_0$ obtained using equation (14). The thick solid line indicated $\alpha_{\max}/{}_f\alpha_0$, when the displacement controller in the case of ${}_d\delta_{\max}/\delta_0$ = 0.2 and 0.4 was in effect, and indicated the range ${}_s\alpha_y/{}_f\alpha_0 > 0$.

Fig. 8(a) and 8(b) show the relationship between $\alpha_{\max}/{}_f\alpha_0$ and $\delta_{\max}/{}_f\delta_0$, with the same analysis values. The thick dashed line represented $\alpha_{\max}/{}_f\alpha_0$, when the displacement controller was not incorporated. The monotonously increasing thin solid line in the upper right part represented ${}_f\alpha_{\max}/{}_f\alpha_0$, obtained from equation

(13), and the decreasing thin solid line in the lower right part represented ${}_s\alpha_y / {}_f\alpha_0$. The thick solid line indicated $\alpha_{\max} / {}_f\alpha_0$, when the displacement controller in the case of ${}_d\delta_{gap} / {}_f\delta_0 = 0.2$ and 0.4 was in effect, and indicated the range of ${}_s\alpha_y / {}_f\alpha_0 > 0$. ▽, ○, and □ in Fig. 7 and 8 indicate the analysis results. When the white legend was ${}_d\delta_{\max} / \delta_0 = 0.4$, the solid legend showed the analysis value when ${}_d\delta_{gap} / {}_f\delta_0 = 0.2$. ▽, ○, and □ showed the analysis value for ${}_{fd}\kappa = 1.0$, 4.0, and 20, respectively.

It can be observed from Fig. 7, 8(a), and 8(b) that the response prediction formula was similar to the analysis value by ART KOBE and ART SHIN, and the evaluation of safety side was mostly found to exceed the analyzed value. In addition, when the displacement controller was not working, an optimum value was obtained, that minimized the maximum shear $\alpha_{\max} / {}_f\alpha_0$, from the prediction equation for $n_1 = 1.0$. Further the obtained value was observed to be minimum, when ${}_s\alpha_y / {}_f\alpha_0 = 0.28$ and ${}_f\alpha_{\max} / {}_f\alpha_0 = \delta_{\max} / {}_f\delta_0 = 0.38$, and $\alpha_{\max} / {}_f\alpha_0 = 0.66$. Similarly, for $n_1 = 10$, $\alpha_{\max} / {}_f\alpha_0 = 0.22$ became the minimum value, when ${}_f\alpha_{\max} / {}_f\alpha_0 = \delta_{\max} / {}_f\delta_0 = {}_s\alpha_y / {}_f\alpha_0 = 0.11$. The prediction equation and the analyzed value of ART KOBE for $n_1 = 1.0$ showed that the deformation optimized before $\delta_{\max} / {}_f\delta_0 = 0.38$. Further, when the deformation of the displacement controller started to work at ${}_d\delta_{gap} / {}_f\delta_0 = 0.2$, the maximum shear force $\alpha_{\max} / {}_f\alpha_0$ was observed to sharply increase. Moreover, when ${}_d\delta_{gap} / {}_f\delta_0 = 0.4$, the displacement controller worked after exceeding the deformation and optimized, and the maximum shear force $\alpha_{\max} / {}_f\alpha_0$ was found to rapidly increase. In the predicted value for $n_1 = 10$ and the analyzed value of ART SHIN, the deformation control mechanism worked after the deformation $\delta_{\max} / {}_f\delta_0 = 0.11$, which was the optimum value for both ${}_d\delta_{gap} / {}_f\delta_0 = 0.2$ and 0.4. Additionally, maximum shear force $\alpha_{\max} / {}_f\alpha_0$ was observed to increase sharply. Further, it was observed that the larger the proportion of the

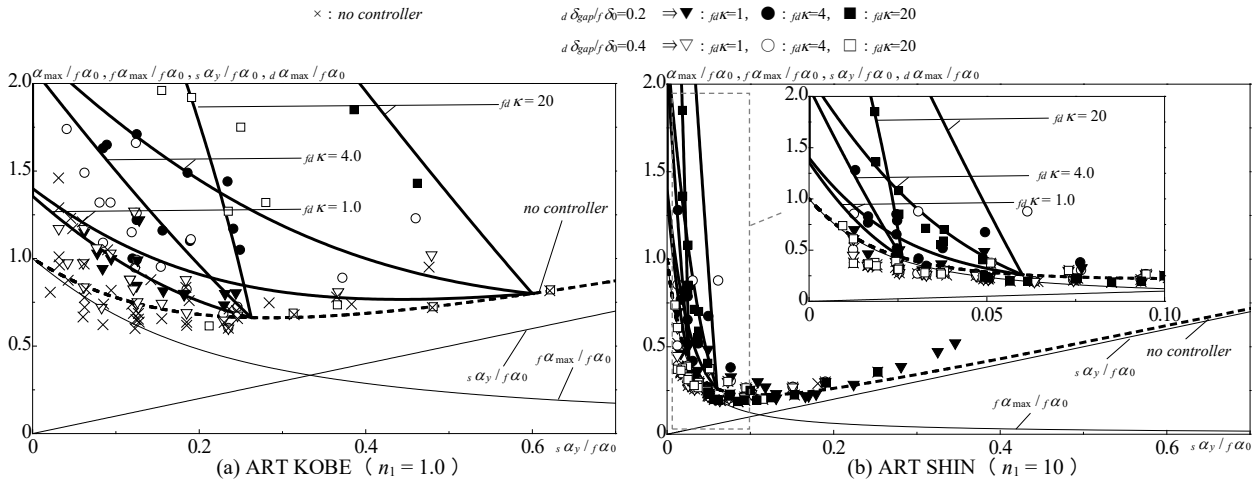

Fig. 7 – Relationship of ${}_s\alpha_y / {}_f\alpha_0$ and $\alpha_{max} / {}_f\alpha_0$

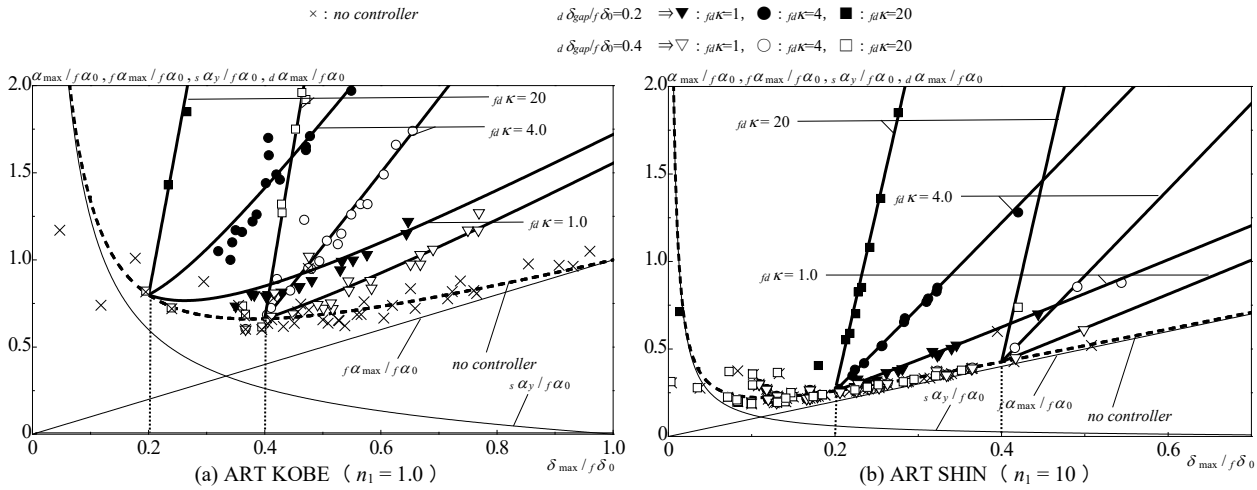

Fig. 8 – Relationship of $\alpha_{max} / {}_f\alpha_0$ and $\delta_{max} / {}_f\delta_0$

stiffness of the flexible element to the stiffness of the displacement controller ${}_{fd}\kappa$, the larger the deformation suppression effect, and a significant increase was also observed in the response shear force $\alpha_{\max}/{}_{f}\alpha_0$.

The results indicated that even when a same maximum deformation was to be controlled, the stiffness of the displacement controller remained small. Further, a sudden increase in the maximum shear force, acting on the main frame, could be suppressed using a method, where the displacement controller acted from a small deformation. However, the range in which the seismic isolation effect could be fully exerted would be reduced. On the other hand, the displacement controller started to work on a large amount of deformation, and the method of increasing the stiffness of the displacement controller widened the range in which the effect of the base isolation structure could be sufficiently exerted. It was quantitatively examined that the maximum shear force of the main frame stiffness increased, when the displacement controller worked.

4. Outline of the displacement control structure model for SDOF and the discussion

In this section, we show an outline method of SDOF base-isolated structure model, with displacement controller, as an example for verification.

4.1 Outline discussion method of the displacement controller for the SDOF system

The following is the outline method of the base-isolated structure with displacement controller for the SDOF system.

Step 1: The parts of the building are set. < Parts of the building >

M: superstructure mass and ${}_{f}T_1$: period of isolation layer

Step 2: The damper is selected, with optimal maximum deformation and maximum shear reduction, for twice the ground motion level 2. < Parts of the damper >

${}_{s}\alpha_y$: yield shear coefficient of the damper

Step 3: The design criteria are set for twice the ground motion level 2 and the parameters of the displacement controller that satisfy the design criteria are determined.

< Design criteria > $\delta_{\max}$: maximum deformation and $\alpha_{\max}$: maximum shear coefficient

< Parts of the displacement controller > ${}_{d}\delta_{gap}$: deformation at which the displacement controller starts to work and ${}_{fd}\kappa$: proportion of the stiffness of the displacement controller to the stiffness of the rubber

4.2 Parameter outlines

The parameters for the displacement controller can be set, such that the response for two times of the ground motion level 2 is satisfied. This can be done using equation (14), which established the relationship between the maximum deformation $\delta_{\max}$ and yield shear coefficient of the stiff element ${}_{s}\alpha_y$, and equation (15), which established the relationship between the shear coefficient of the main frame $\alpha_{\max}$ and the yield shear coefficient of the stiff element ${}_{s}\alpha_y$,. Moreover, we can also study the relationship between the deformation and shear of the displacement controller using previous discussions. Further, it is necessary to select ${}_{d}\delta_{gap}$, as shown in the previous section, where outlines were discussed. Therefore, in the study, ${}_{d}\delta_{gap}$ was directly set as the parameters of the displacement controller. Table 2 shows the analysis parameters used in this study. In

Table 2 – Analytical parameter

${}_{f}T_1$	${}_{s}\alpha_y$	${}_{d}\delta_{gap}$ (cm)	${}_{fd}k$	V_E (V_D) (cm/s)
4.0	0.01, 0.02, 0.04, 0.06, 0.10	10, 20, 30,40	10, 20	120(98), 240(195), 360(293)

the seismic isolation structure model, the period of the isolation layer was ${}_{f}T_1$=4.0 s. V_D, shown in the bracket

in table 2, is calculated using the following equation [12].

$$V_D = \frac{V_E}{1+3\,{}_f h+1.2\sqrt{{}_f h}} \tag{17}$$

Here, ${}_f h$: The damping ratio of the main frame.

4.3 Displacement controller model for SDOF system

Fig. 9 shows the relationship between the maximum shear $\alpha_{\max}$ and maximum deformation $\delta_{\max}$, based on the predicted values of the SDOF isolation structure system model, with displacement controller. Fig. 9 shows the predicted values when the specifications of the displacement controller were changed for each ${}_s\alpha_y$ (Table 1). When the displacement controller was not incorporated (in Fig. 9, it is expressed as "no controller"), it was represented by a broken line. The level 2 ground motion (hereafter referred as V_E = 120 cm/s) and the two times level 2 ground motion (hereafter referred as V_E = 240 cm/s) were shown for the range of ${}_s\alpha_y$ = 0.01–0.15. Further, when the displacement controller was not working, the predicted values of V_E = 120 cm/s and V_E = 240 cm/s in each ${}_s\alpha_y$ were observed to be connected by dotted lines, and the plot represented ${}_s\alpha_y$. Moreover, when the displacement controller was working, it was represented by a solid line. The base isolation model showed the predicted values for V_E = 240 cm/s, within the ${}_s\alpha_y$ range of 0.01–0.10. The transition of the predicted value, when ${}_s\alpha_y$ and ${}_{fd}\kappa$ were constant and ${}_d\delta_{gap}$ changed, and the transition of the predicted value, when ${}_d\delta_{gap}$ and ${}_{fd}\kappa$ were constant, were plotted and the plot showed ${}_d\delta_{gap}$. For ${}_{fd}\kappa$ and ${}_d\delta_{gap}$, ${}_{fd}\kappa$ = 10 and 20, and ${}_d\delta_{gap}$ shown in the plot were ${}_d\delta_{gap}$ = 10, 20, 30, and 40 cm, respectively (see Table 2). Fig. 10 shows the results of the predicted values and the analyzed values, for the case that satisfied the design criteria, obtained from the schematic study of the SDOF displacement controller structure model.

The seismic isolation structure model is described in Fig. 9 and 10. It can be observed from Fig. 9 that for selecting the optimum damper amount for Level 2 earthquake motion and considering the results for V_E = 120 cm/s, $\alpha_{\max}$ was observed to be reduced in the range of ${}_s\alpha_y$ = 0.02–0.06. From this, we selected ${}_s\alpha_y$ = 0.02 as the optimum amount of damper for Level 2 earthquake motion. The design criteria for the seismic motion at two times level 2 were $\delta_{\max}$ = 60 cm and $\alpha_{\max}$ = 1.0, and the results for V_E = 240 cm/s of the base isolation structures, with ${}_s\alpha_y$ = 0.02, exceeded for $\delta_{\max}$ = 60 cm. Therefore, the specifications of the displacement controller were determined, such that $\delta_{\max}$ was reduced by incorporating the displacement controller and an increase in $\alpha_{\max}$ also satisfied the design criteria. It can be observed from Fig. 9 that the design criteria were satisfied by incorporating the displacement controller as ${}_d\delta_{gap}$ = 30 cm and ${}_{fd}\kappa$ = 10 displacement control mechanism into the base isolation structure of ${}_s\alpha_y$ = 0.02. Fig. 10 shows the results of a general study focusing on the cases ${}_s\alpha_y$ = 0.02, ${}_d\delta_{gap}$ = 30 cm, and ${}_{fd}\kappa$ = 10. Fig. 10 shows that the predicted values were mostly similar to the analyzed values on the safety side.

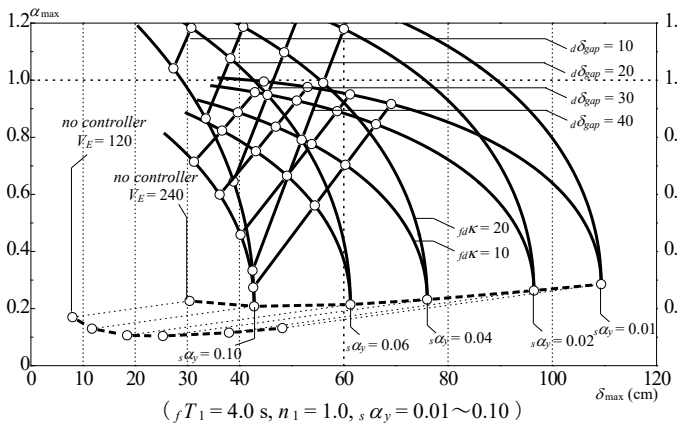

Fig. 9 – Consideration of the displacement controller model with SDOF

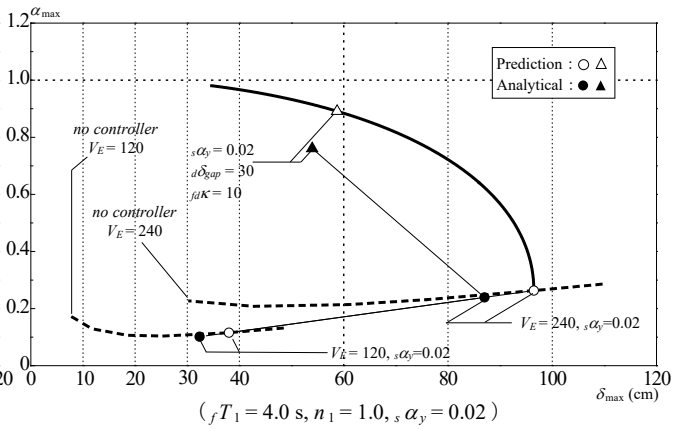

Fig. 10 – Consideration results of the displacement controller model with SDOF

From results, it was possible to qualitatively and easily evaluate the response characteristics of the SDOF displacement control structural model by using the proposed response prediction equation.

4.4 Discussion on the response characteristics of one mass system deformation control model

The response characteristics of the displacement controller structure were considered with reference to Fig. 9. Based on the results of the deformation control structure, shown in Fig. 9, the maximum deformation was reduced by incorporating the displacement controller, and the decreasing tendency became more prominent as ${}_{fd}\kappa$ increased and ${}_{d}\delta_{gap}$ decreased in the range where the damper amount was small. It can be seen from this result that excellent maximum deformation reduction effect was obtained by selecting an optimal damper amount for the ground motion of level 2 and incorporating the displacement controller in the seismic isolation structure with the damper amount. However, as the maximum deformation was observed to be reduced, while the maximum shearing force was observed to be increased, the maximum deformation reduction effect of the deformation control mechanism reached a limit. It was necessary to set appropriate parameters for the displacement controller with respect to the maximum shear force. Also, by using the result shown in Fig. 9 (without displacement controller), it was possible to reduce the maximum deformation without incorporating the displacement controller by increasing the amount of damper in the seismic isolation structure from. However, increasing the amount of damper by assuming the effect of reducing the response to large-level ground motions, with a low probability of occurrence, was not found to be efficient and economical in terms of damper performance for small-level ground motions.

As described above, it was considered significantly important to combine the selected damper with a displacement controller and increase the amount of damper for level 2 ground motions for reducing the maximum deformation of the base-isolated structure in case of maximum earthquakes. It was also observed that when the displacement controller was incorporated, the maximum shear force increased owing to the maximum deformation reduction effect, and when the damper amount was increased, the damper efficiency decreased for small ground motion levels. Therefore, it was considered that an appropriate mechanism needs to be incorporated per the required performance of the building.

5. Summary

The purpose of this study was to qualitatively and easily evaluate the response characteristics of a displacement controller structure that incorporated a displacement controller, with hardening-type restoring force characteristics, into a seismic isolation structure used as a building with advanced seismic performance. We extended the seismic design method, based on the energy balance proposed for an SDOF model, onto the displacement controller structure that incorporated the displacement controller in a flexible–stiff mixed structure, and proposed an energy method for the displacement controller structure. In addition, the response prediction formula was verified using the time history response analysis.

(1) In this study, a displacement controller structure was considered. This incorporated a displacement controller exhibiting a hardening-type restoring force characteristic of a stiff element in a flexible–stiff mixed structure, which consisted of a flexible element that exhibited elastic behavior and a stiff element that exhibited elastic-plastic behavior. Based on the assumption that all deformation contributes to the deformation of the damper, a response prediction formula for the SDOF model was derived.

(2) The predicted values were confirmed by comparing the result parameters of the time-history response analysis and predicted values of the response. The parameters were as follows: ${}_{f}T_1$ was the flexible element 1 natural period, ${}_{d}\delta_{gap}/{}_{f}\delta_{y}$ was the deformation at which the displacement control begins to function, ${}_{f}k$ was the stiffness of the flexible element, ${}_{d}k$ was the stiffness of the displacement control, ${}_{fd}\kappa$ was the proportion of ${}_{f}k$ to ${}_{d}k$, E_D was energy contributing to the damage, and V_D was the speed conversion value of E_D. Thus, the tendency of the response characteristics of the displacement controller structure was evaluated by using the proposed response prediction formula.

(3) The response prediction equation, based on the energy balance in the displacement controller structure,

indicated excellent reduction tendency of the maximum deformation $\delta_{\max}/{}_f\delta_0$, as the stiffness ${}_{fd}\kappa$ of the displacement controller was found to be larger and the deformation ${}_d\delta_{gap}/{}_f\delta_0$ at which the displacement controller starts to work was found to be smaller. Further, it was observed that the larger the stiffness ${}_{fd}\kappa$ of the displacement controller, the higher the tendency of the maximum shear force $\alpha_{\max}/{}_f\alpha_0$ to increase.

(4) In this paper, the outline examination method and examination example for the SDOF model of the displacement control structure, assuming the base-isolation structure, were also described. It was shown that the response characteristics, when the controller was incorporated in each structure, could be evaluated by using the values obtained from the proposed response prediction formula and by analyzing.

(5) The maximum deformation of the base-isolated structure was observed to be reduced in case of a maximum earthquake, by combining the damper and deformation control mechanism selected for level 2 ground motion and increasing the amount of damper. However, owing to some issues, the importance of proper selection of structural combinations for structural performance requirements was revealed. One problem was that when the displacement controller was incorporated, the maximum shear force increased owing to maximum deformation reduction effect, and when the damper amount increased, the damper efficiency was reduced with respect to a small ground motion level.

References

[1] Harada Y., Akiyama H. (1995): Seismic design of flexible-stiff mixed frame with energy concentration. *AIJ Journal of Structural Engineering 1995/06*, **60** (472), 57-66.

[2] Akiyama H. (1995): Earthquake resistant design to meet to diversified performance. *AIJ Journal of Structural Engineering 1995/06*, **60** (472), 85-90.

[3] AIJ (1995): Preliminary reconnaissance report of the 1995 Hyogoken-Nanbu earthquake. 6-26.

[4] AIJ (2011): Preliminary reconnaissance report of the 2011 Tohoku-Chiho Taiheiyo-Oki earthquake. 16-27.

[5] AIJ (2011,2013): Public research meeting on long-period ground motion countermeasures. 2011, 39-138, 2012, 94.

[6] Cabinet Office Japan, Tokyo near-field earthquake management , http://www.bousai.go.jp/jishin/syuto/index.html.

[7] ANUNHT, JISF, JSSC (2009): New structural system building research and development project using innovative structural materials collaborated with the ministry (Proposal) 2009, 1-6.

[8] Kobori T., Minai R. (1956): Seismic design of flexible-stiff mixed frame with energy concentration. *Architectural Institute of Japan 1956/03*, **60** (52), 41-48.

[9] Takahashi T., Anahara K..: Experimentation and simulation of seismic impact generated in a bade-isolated house by a horizontal displacement control. *AIJ Journal of Structural Engineering 2003/11*, **68** (537), 223-230.

[10] Iiba M., Midorikawa M., Hanai T., Minagawa T. (2004): Effects of displacement restraint device on seismic response of base isolated house with collision at isolated layer (1, 2). *Summaries of technical papers of Annual Meeting, Architectural Institute of Japan E E 2004/08*, 425-428.

[11] Nakata S., Hanai T., Iiba M., Azuhata T. (2007): Study on Safety at The Earthquake of Base-Isolated House with Displacement Control Systems. (1, 2). *Summaries of technical papers of Annual Meeting, Architectural Institute of Japan E E 2007/08*, 1001-1004.

[12] Akiyama H. (1999): Earthquake-Resistant Design Method for Buildings Based on Energy Balance. 1st edition.

[13] Kuribayashi K., Sato D., Kitamura H., Yamaguchi M., Nishimoto K. (2011): Energy balance-based seismic response prediction method for steel structure considering effective hysteretic damper deformation. *AIJ Journal of Structural Engineering 2011/03*, **76** (611), 543-552.

[14] Kitamura H. (2009): Seismic Response Analysis Methods for Performance Based Design. Shokokusha, 2nd edition.

[15] Kitamura H., Zaitsu K., Mayahara T.: Energy balance-based seismic response prediction method for response-controlled building using hysteresis dampers. *AIJ Journal of Structural Engineering 2006/01*, **71** (599), 71-78.

[16] The Japan Society of Seismic Isolation (2009): Seismic Isolation Material Standard List 2009, 1st edition.

